

Effect of cross-phase modulation on supercontinuum generated in microstructured fibers with sub-30 fs pulses

G. Genty, M. Lehtonen, and H. Ludvigsen

Fiber-Optics Group, Department of Electrical and Communications Engineering, Helsinki University of Technology,
P.O. Box 3500, FI-02015 HUT, Finland
goery.genty@hut.fi

Abstract: We investigate the effects of cross-phase modulation between the solitons and dispersive waves present in a supercontinuum generated in microstructured fibers by sub-30 fs pulses. Cross-phase modulation is shown to have a crucial importance as it extends the supercontinuum towards shorter wavelengths. The experimental observations are confirmed through numerical simulations.

©2004 Optical Society of America

OCIS codes: (190.5530) Pulse propagation and solitons; (230.3990) Microstructure devices

References and links

1. J. K. Ranka, R. S. Windeler, and A. J. Stentz, "Visible continuum generation in air-silica microstructure optical fibers with anomalous dispersion at 800 nm," *Opt. Lett.* **25**, 25-27 (2000).
2. See for example *Nonlinear optics of photonic crystals*, Special issue of *J. Opt. Soc. Am. B* **19**, 1961-2296 (2002) or *Supercontinuum generation*, Special issue of *Appl. Phys. B* **77**, 143-376 (2003).
3. G. Genty, M. Lehtonen, H. Ludvigsen, J. Broeng, and M. Kaivola, "Spectral broadening of femtosecond pulses into continuum radiation in microstructured fibers," *Opt. Express* **10**, 1083-1098 (2002), <http://www.opticsexpress.org/abstract.cfm?URI=OPEX-10-20-1083>
4. A. Ortigosa-Blanch, J. C. Knight, and P. S. J. Russell, "Pulse breaking and supercontinuum generation with 200-fs pump pulses in photonic crystal fibers," *J. Opt. Soc. Am. B* **19**, 2567-2572 (2002).
5. M. Lehtonen, G. Genty, M. Kaivola, and H. Ludvigsen, "Supercontinuum generation in a highly birefringent microstructured fiber," *Appl. Phys. Lett.* **82**, 2197-2199 (2003).
6. J. M. Dudley, L. Provino, N. Grossard, H. Maillotte, R. S. Windeler, B. J. Eggleton, and S. Coen, "Supercontinuum generation in air-silica microstructured fibers with nanosecond and femtosecond pulse pumping," *J. Opt. Soc. Am. B* **19**, 765-771 (2002).
7. A. Proulx, J. Ménard, N. Hô, J. M. Laniel, R. Vallée, and C. Paré, "Intensity and polarization dependences of the supercontinuum generation in birefringent and highly nonlinear microstructured fibers," *Opt. Express* **11**, 3338-3345 (2003), <http://www.opticsexpress.org/abstract.cfm?URI=OPEX-11-25-3338>
8. Z. Zhu and T. G. Brown, "Experimental studies of polarization properties of supercontinua generated in a birefringent photonic crystal fiber," *Opt. Express* **12**, 791-796 (2004), <http://www.opticsexpress.org/abstract.cfm?URI=OPEX-12-5-791>
9. N. Nishizawa and T. Goto, "Experimental analysis of ultrashort pulse propagation in optical fibers around zero-dispersion region using cross-correlation frequency resolved optical gating," *Opt. Express* **8**, 328-334 (2001), <http://www.opticsexpress.org/abstract.cfm?URI=OPEX-8-6-328>
10. N. Nishizawa and T. Goto, "Characteristics of pulse trapping by ultrashort soliton pulse in optical fibers across zero-dispersion wavelength," *Opt. Express* **10**, 1151-1160 (2002), <http://www.opticsexpress.org/abstract.cfm?URI=OPEX-10-21-1151>
11. L. Tartara, I. Cristiani, and V. Degiorgio, "Blue light and infrared continuum generation by soliton fission in a microstructured fiber," *Appl. Phys. B* **77**, 307-311 (2003).
12. S. A. Diddams, D. J. Jones, J. Ye, S. T. Cundiff, J. L. Hall, J. K. Ranka, R. S. Windeler, R. Holzwarth, T. Udem, and T. W. Hänsch, "Direct link between microwave and optical frequencies with a 300 THz femtosecond laser comb," *Phys. Rev. Lett.* **84**, 5102-5105 (2000).
13. A. V. Husakou and J. Herrmann, "Supercontinuum generation in photonic crystal fibers made from highly nonlinear glasses," *Appl. Phys. B* **77**, 227-234 (2003).
14. A. V. Husakou and J. Herrmann, "Supercontinuum generation, four-wave mixing, and fission of higher-order solitons in photonic-crystal fibers," *J. Opt. Soc. Am. B* **19**, 2171-2182 (2002).
15. G. P. Agrawal, *Nonlinear Fiber Optics*, 3rd ed. (Academic Press, New York, 2001).

16. P. Beaud, W. Hodel, B. Zysset, and H. P. Weber, "Ultrashort pulse propagation, pulse breakup, and fundamental soliton formation in a single-mode optical fiber," *IEEE J. Quantum Electron.* **23**, 1938-1946 (1987).
 17. H. A. Haus and E. P. Ippen, "Group velocity of solitons," *Opt. Lett.* **26**, 1654-1656 (2001).
 18. N. Nishizawa and T. Goto, "Widely broadened super continuum generation using highly nonlinear dispersion shifted fibers and femtosecond fiber laser," *Jpn. J. Appl. Phys.* **40**, L365-L367 (2001).
 19. I. Cristiani, R. Tediosi, L. Tartara, and V. Degiorgio, "Dispersive wave generation by solitons in microstructured optical fibers," *Opt. Express* **12**, 124-135 (2004), <http://www.opticsexpress.org/abstract.cfm?URI=OPEX-12-1-124>
-

1. Introduction

Supercontinua (SC) can be generated by launching pulses with a high peak power into narrow-core microstructured fibers (MFs) [1,2]. The complex mechanisms behind the extremely broad spectra obtained have been investigated by several research groups for various input-pulse characteristics, such as wavelength [3-5], temporal width [5,6], peak power, and polarization [5,7,8]. The interplay between the optical properties of the MFs, e.g., dispersion and fiber length, and the physical phenomena have also been analyzed [1,3]. Among the various nonlinear processes, the generation of strong blue spectral components with femtosecond pulses at wavelengths falling in the anomalous dispersion region of the MF has received considerable attention. Nevertheless, the commonly given explanation of the dispersive-wave generation fails to fully predict the spectral distribution of the blue components. In particular, the SC spectrum extends further to the blue than predicted by requiring phase-matching between the dispersive waves and the multiple solitons that result from the decay of the initial pulses. Also, the experimentally measured amplitude of the blue spectral components has been found to be surprisingly large. Recently, it has been suggested that pulse trapping between the solitons and the dispersive waves could explain the observed features [9-11].

In this paper, we investigate the physical phenomena responsible for the formation of the blue components in the SC spectrum generated when launching sub-30 fs pulses into a narrow-core MF. We demonstrate that in our experiments cross-phase modulation (XPM) is an important factor which causes new spectral lines to be created on the short-wavelength side and thereby extending the spectrum further towards the blue. We can not confirm the results of Refs. [9-11] suggesting that this would be due to pulse trapping and shift of the carrier frequency of the dispersive wave in order to match the group velocities of the dispersive and solitons waves. Rather, we suggest that the continuous blue shift results from cascaded XPM occurring as the solitons and the dispersive waves travel at different group velocities. The high dispersion at the wavelength of the dispersive waves also shows to play a crucial role. We present a detailed analysis of the phenomenon through numerical simulations and compare the findings with experimental data. Finally, we discuss the effect of XPM in the context of SC generation with longer 200-fs pulses and show that they are in agreement with reported experimental observations.

2. Experiments

The pump source used for generating the supercontinua was a Ti:Sapphire laser (Giga-Optics/Gigajet Kit 20) producing 27 fs pulses at a repetition rate of 1 GHz. The center wavelength of the pulses is located at 790 nm and the maximum average power of the output was 600 mW. This type of a laser has been widely used for generating the frequency combs for optical frequency metrology [12]. The pulses were coupled into the MF using an achromatic lens with a 2-mm focal length yielding a coupling efficiency of ca. 20%. The 1.5 m long MF had a core diameter of 1.67 μm and an air-filling fraction of 63%. The dispersion of the fiber as a function of wavelength is displayed in Fig. 1.

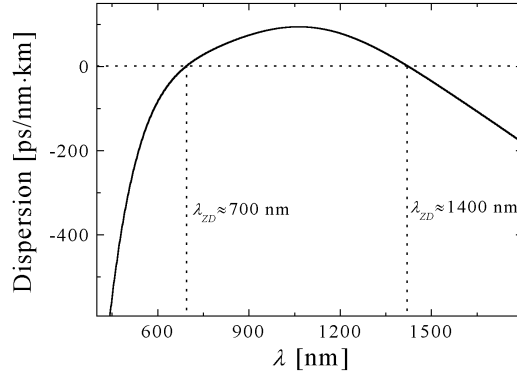


Fig. 1. Dispersion profile of the microstructured fiber. λ_{ZD} : zero-dispersion wavelength.

The fiber has two zero-dispersion wavelengths, one located at around 700 nm and another at 1400 nm. The fiber exhibits large birefringence which, for input pulses polarized along one of the principal axes, results in a polarized continuum [5,7]. Single-mode behavior of the MF was observed for wavelengths above at least 400 nm. Spectra of the continuum generated in the MF for increasing input power are presented in Fig. 2. For the highest average input power of ~120 mW, the spectrum extends from 450 nm to 1600 nm.

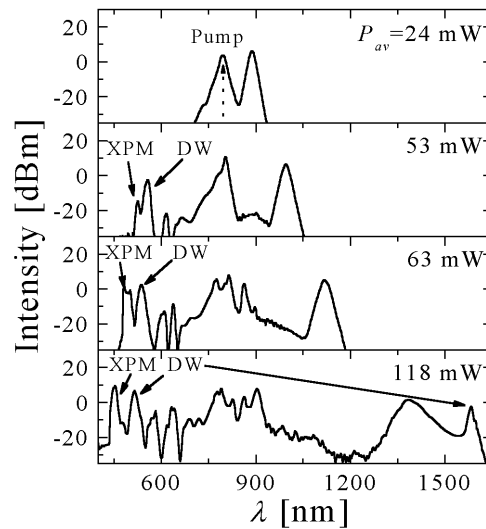


Fig. 2. Supercontinuum spectra recorded at the output of the MF for increasing average input power. P_{av} : average power, XPM: cross-phase modulation, and DW: dispersive wave. $\lambda_p=790$ nm and $\Delta\tau=27$ fs.

For low input power two distinct spectral peaks are observed. The peak shifted most to the red corresponds to a soliton experiencing soliton-self frequency shift (SSFS) as previously reported by several authors [3-6]. As the input power is increased, the red-shift of the soliton is considerably enhanced with the simultaneous appearance of blue components in the spectrum. The peak marked with DW in Fig. 2 corresponds to a dispersive wave. The location of this peak slightly varies with the input power. Besides, a new spectral peak marked with XPM and located on the blue edge of the spectrum appears as the input power is increased. The magnitude of the XPM peak increases and its wavelength decreases with increasing input power. The wavelength separation between this new peak and the DW peak with the lowest wavelength also increases. On the infrared side, the distinct peak at around 1600 nm seen in

the lowest spectrum also results from the generation of a dispersive wave beyond the infrared λ_{ZD} [13].

3. Analysis

The onset of the continuum formation can be explained in the framework described in earlier publications [3-5]. As a result of the interplay between self-phase modulation and anomalous dispersion, the input pulse is first compressed, which leads to an expansion of the spectrum into the normal dispersion region of the fiber. The spectral overlap between the pulse and a dispersive wave (DW) with the same wave vector results in the generation of the DW. As a result there appears a distinct peak in the blue region of the spectrum indicated by the DW-arrow in Fig. 2. The location of the DW peak in the spectrum can be found from the phase-matching condition [14]

$$\Delta\beta = \beta(\omega_p) - \beta(\omega_{DW}) = (1 - f_R)\gamma(\omega_p)P_p - \sum_{n \geq 2} \frac{(\omega_{DW} - \omega_p)^n}{n!} \beta_n(\omega_p) = 0, \quad (1)$$

where $\beta(\omega_p)$ and $\beta(\omega_{DW})$ denotes the propagation constants of the MF at the angular frequencies of the pump and the dispersive wave, respectively, and γ is the nonlinear coefficient of the MF and β_n denotes the n^{th} term in the Taylor-series expansion of the propagation constant at around ω_p . The factor f_R accounts for the fractional contribution of the Raman-delayed response of the fiber and P_p is the peak power of the compressed pulse (and not to that of the initial input power). In our case, the peak power of the pulse is roughly doubled after compression [15]. The phase-matching condition of Eq. (1) is plotted in Fig. 3 as a blue solid line using the full propagation constant of our fiber and for a pump wavelength of 790 nm and an initial average power of 120 mW (corresponding to $P_{p, \text{initial}} = 3.6$ kW). For comparison, the spectrum recorded at the output of the MF is also shown.

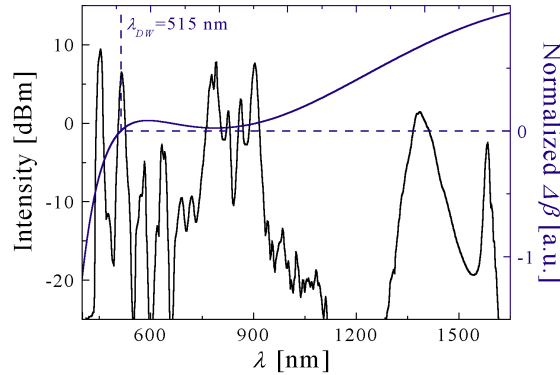


Fig. 3. Phase-matching condition for the generation of the dispersive wave (blue line). The SC spectrum is displayed as a black line. $P_{av} = 118$ mW, $\lambda_p = 790$ nm, and $\Delta\tau = 27$ fs. λ_{DW} denotes the wavelength of the dispersive wave calculated from Eq. (1).

The location of the dispersive wave at 515 nm is well predicted by Eq. (1). Furthermore, Fig. 3 shows that the peak located at the blue edge of the spectrum should not result from the generation of a dispersive wave, since its location is detuned by more than 60 nm from the phase-matched 515 nm.

To clarify the origin of the left-most peak near 450 nm in the spectrum of Fig. 3, we model the propagation of a 27 fs pulse along the MF using the nonlinear Schrödinger equation [15]. In order to accurately simulate our experiments, the full propagation constant of the MF is included together with the Raman contribution and the self-steepening effect. The variation of the effective area of the fiber with wavelength and the wavelength-dependent losses are also taken into account in the model. The simulated spectrum is illustrated in Fig. 4. It resembles the measured one to a great extent. In particular, the spectrum of the solitons and

the location of the blue peaks are faithfully reproduced. The peak at around 1600 nm appears to be broader in the simulation than in the experiments. This could be due to the leakage losses being underestimated at long wavelengths. Besides, the simulation indicates that the blue spectral components contain about 10% of the total energy, which is less than the 22% estimated from the experimental data shown in Fig. 3. This discrepancy could be due to the drop of the spectral intensity at longer wavelengths resulting from the decreasing sensitivity of the spectrum analyzer.

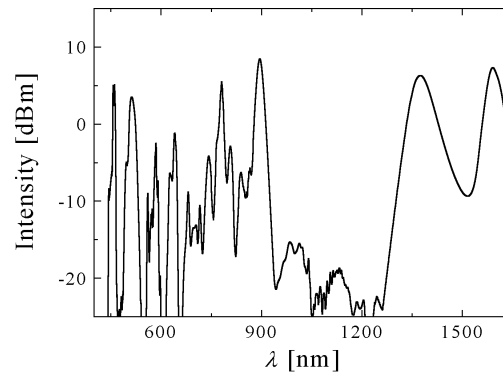


Fig. 4. Simulated SC spectrum. The parameters of the input pulse are the same as in the experiment shown in Fig. 3. For better comparison, the simulated spectrum was averaged over the same spectral window as is the resolution bandwidth of the optical spectrum analyzer applied in the experiments, i.e., 10 nm.

The simulated spectrogram of the supercontinuum is displayed in Fig. 5 for different propagation lengths along the fiber. A pump pulse with a peak power of P_p and full-width at

half-maximum of T_{FWHM} decays into N solitons as $N = \sqrt{\frac{\gamma P_p}{1.76 \beta_2}} T_{FWHM}$, where γ and β_2 are

the nonlinear coefficient and the dispersion value at the pump wavelength, respectively. A visible dispersive wave is initially generated at a wavelength determined by Eq. (1) (see Fig. 5(a)). The simulation shows that the location of the dispersive wave is independent of the propagation distance as could be expected from Eq. (1). From Fig. 5, it is also clear that as the center wavelength of the soliton shifts with propagation, its spectrum does not extend anymore beyond the visible zero-dispersion wavelength and, therefore, does not generate new dispersive waves along propagation. Even though the pump and the blue dispersive wave initially have the same phase, the dispersive wave travels at a slower velocity than the pump making these two waves to separate in time from each other. The first soliton which splits off from the pump carries most of the power. With propagation it experiences the SSFS and its center wavelength shifts towards the red. Consequently, the soliton group velocity decreases. This decrease results in a progressive catching up of the soliton by the blue dispersive wave. When the soliton walks through the dispersive wave, spectral components on a blue side of the dispersive wave start to appear (see Figs. 5(b)-(c)). These components move at a different group-velocity than the soliton and the dispersive wave and they disperse with further propagation along the MF (see Fig. 5(d)). Also, interaction between the newly generated blue components and the soliton is observed (see Fig. 5(c)). The spectrum of the soliton is not affected by the co-propagation of the dispersive wave. Furthermore, as the spectrum of the soliton extends into the normal dispersion region beyond 1400 nm an infrared dispersive wave is generated (see Fig. 5(d)). The interaction between the soliton and the infrared dispersive wave differs from that of the soliton and the blue dispersive wave. In particular, the infrared dispersive wave travels with a faster group velocity than the soliton and, therefore, these two cannot cross.

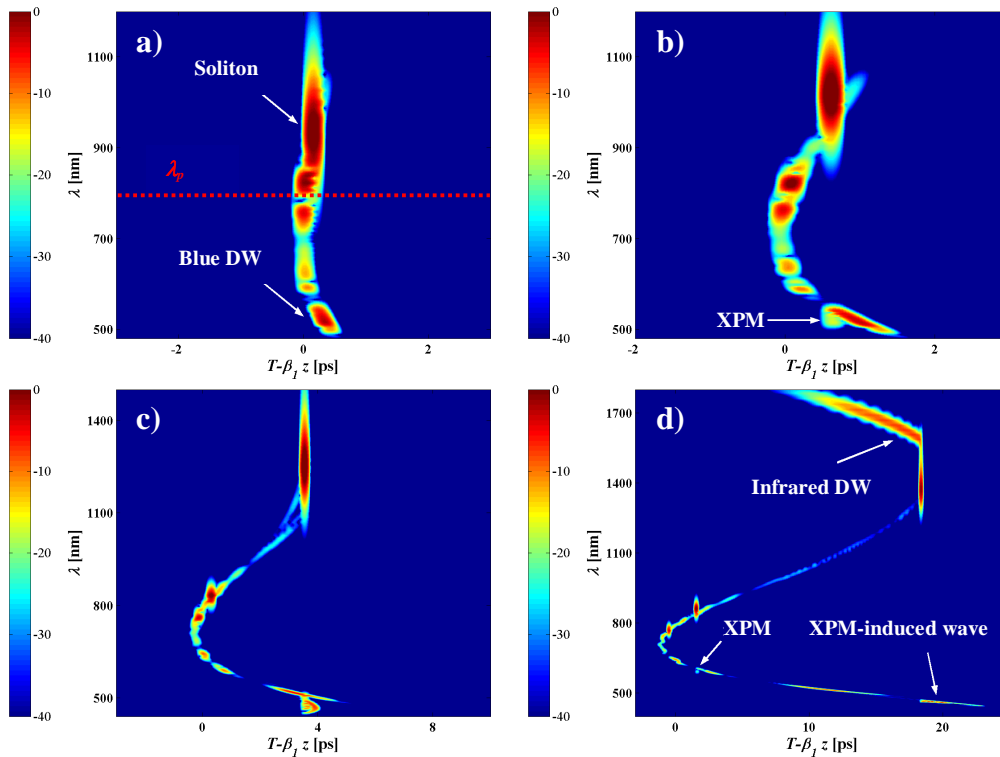


Fig. 5. Simulated spectrogram of the continuum after a) 2 cm, b) 5cm, c) 15 cm and d) 50 cm of propagation along the MF. DW: dispersive wave. $P_{av}=118$ mW, $\lambda_p=790$ nm, and $\Delta\tau=27$ fs.

As the soliton and the blue dispersive wave temporally overlap over a distance δz in the fiber, the soliton induces a time-dependent nonlinear cross-phase change $\delta\phi_{XPM}$ on the dispersive wave [15]

$$\delta\phi_{XPM}(T) = 2\gamma(\omega_{DW})|A(T - \Delta\beta_1 z)|^2 \delta z = 2\gamma(\omega_{DW})P_S(z) \operatorname{sech}\left(\frac{T - \Delta\beta_1 z}{T_S(z)}\right)^2 \delta z, \quad (2)$$

where A , P_S , and T_S represent the amplitude, peak power and temporal width of the soliton at the distance z , respectively. The walk-off of the soliton and the blue dispersive wave is accounted for through their group-delay difference $\Delta\beta_1$. The nonlinear phase change is directly proportional to the nonlinear coefficient γ at the frequency of the dispersive wave ω_{DW} . Note that the peak power, width and group-delay of the soliton vary with the propagation length z due to the SSFS which induces a constant reshaping of the soliton. The peak power of the dispersive wave is much lower than that of the soliton and, therefore, the XPM induced by the dispersive wave on the soliton is negligible. For the same reason, the nonlinear phase change induced by the dispersive wave on itself (self-phase modulation) is also negligible compared to $\delta\phi_{XPM}$.

The nonlinear phase change induced by the soliton on the dispersive wave affects considerably the propagation of the dispersive wave. In the early stage, the trailing edge of the soliton pulse interacts with the leading edge of the dispersive wave and generates positive chirp, i.e., blue-shift. Therefore, the leading edge of the dispersive wave consists of blue-shifted spectral components which, due to the normal dispersion of the MF at these wavelengths, travel slower than the red components of the dispersive waves. The initially positive quasi-linear frequency chirp of the dispersive wave which shows as a tilt in the

spectrogram (see Fig. 5(a)), strongly affects the dynamics of the XPM between the soliton and the dispersive wave as illustrated in Fig. 6. Indeed, the blue part of spectral component created by XPM appears to be shifted further into the blue as the soliton is delayed whereas the red part becomes less and less visible, since it overlaps with the leading edge components of the dispersive wave. Moreover, due to the high dispersion value at the wavelength of the dispersive wave, the dispersion length of the dispersive wave is small compared to the walk-off length of the soliton and the dispersive wave. As a consequence, dispersion of the XPM-induced spectral components cannot be neglected. In particular, the blue-shifted XPM components are generated first, since the leading edge of the dispersive wave first overlaps with the trailing edge of the soliton (see Fig. 6(b)) and they experience dispersion with further propagation (see Figs. 6(d)-(f)). This prevents the positive chirp induced by the trailing edge of the soliton to be fully compensated for by the negative chirp induced by its leading edge and as a net result one observes an enhanced blue-shift of the XPM components. Cross-phase modulation does not involve any energy exchange between the soliton and the dispersive wave and manifests itself as the spectral redistribution of the energy of the dispersive wave. This explains the fact that the spectral bandwidth of the dispersive wave decreases on the red side as the blue spectral components are generated. In addition, the newly created blue-shifted components travel at slower and slower group velocities inducing the bow-like shape observed in the spectrograms (see Figs. 6(c)-(e)). With further propagation, the group velocity of the soliton decreases and it overlaps not only with the dispersive wave but also with those newly created blue components. The cascaded XPM leads to an even larger blue-shift and as for XPM interaction between the dispersive wave and the soliton, the XPM interaction between the soliton and the XPM-induced blue spectral components results in a redistribution of the energy towards the blue. This explains the gap observed between the dispersive wave and the XPM-induced blue components which appear in the spectrum at the output of the fiber as a distinct peak in Figs. 3-4. The magnitude of this peak and its wavelength-separation from the dispersive wave peak is an increasing function of the input power as could be observed in the experiments (see Fig. 2). An increase in the input power leads to an increase in the peak power of the soliton thus enhancing the XPM interaction (see Eq. (2)).

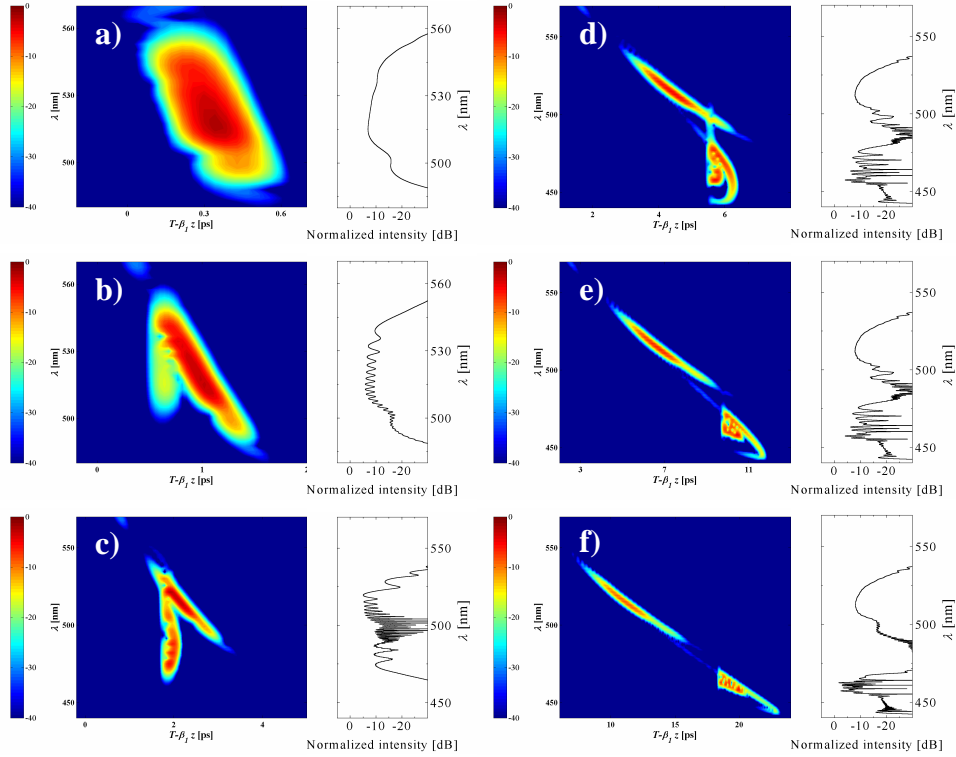


Fig. 6. Spectrogram and corresponding spectrum of the blue dispersive wave after a) 2 cm, b) 5 cm, c) 10 cm, d) 20 cm, e) 30 cm and f) 50 cm of propagation in the fiber.

The XPM effects described above can conveniently be visualized in the spectrogram animation presented in Fig. 7.

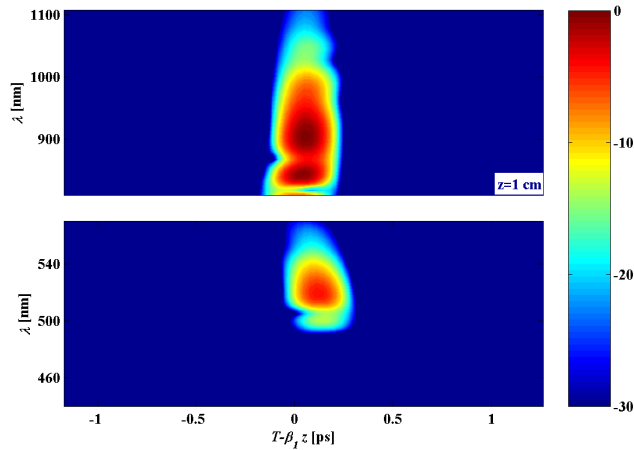


Fig. 7. Spectrogram animation of the soliton and dispersive wave.

As the soliton experiences the SSFS, its width increases due a change in the dispersion and its peak power decreases. This, in turns, reduces the magnitude of $\delta\phi_{XPM}$ (see Eq. (2)) and thereby the efficiency of the XPM blue-shift as is seen in Fig. 6. Furthermore, it is clear from the simulations that no such pulse trapping and shift of the dispersive wave carrier frequency for

group velocity matching with the soliton as described in Refs. [9-11] can be observed here. The XPM-induced blue spectral components disperse with propagation. The XPM interaction ceases as soon as the soliton has walked through the dispersive wave.

To confirm that the effects described above are indeed induced by XPM, the evolution of the dispersive wave along the fiber was simulated by solving the simplified nonlinear Schrödinger equation in a frame of reference moving at the group velocity of the dispersive wave. Only the dispersion, the XPM induced by the soliton and the group-delay difference between the soliton and the dispersive wave are included in the equation

$$\frac{\partial B}{\partial z} + \Delta\beta_1 \frac{\partial B}{\partial T} + i \frac{\beta_2(\omega_{DW})}{2} \frac{\partial^2 B}{\partial T^2} = i\varphi_{XPM}. \quad (3)$$

Here B represents the amplitude of the dispersive wave, $\Delta\beta_1$ is the group-delay difference between the soliton and the dispersive wave, and β_2 is the dispersion coefficient at the frequency of the dispersive wave ω_{DW} . The term φ_{XPM} on the right-hand side of Eq. (3) accounts for the XPM induced by the soliton on the dispersive wave as is defined by Eq. (2). Due to the low peak power of the dispersive wave and the high dispersion value, self-phase modulation is not expected to play a major role in the evolution of the dispersive wave and is therefore not included in Eq. (3). This assumption was actually checked by adding the self-phase modulation term in the simulation. No change in the results was observed.

To take into account the SSFS experienced by the soliton, its characteristics (peak power, temporal width, and group-delay) are evaluated after each propagation step δz by following the procedure described in Ref. [16]. The new values obtained for P_s , T_s , and $\beta_1(\omega_s)$ are then utilized for calculating φ_{XPM} after the dispersive wave has propagated over a distance δz . In principle, a corrective term should be added to the value of $\beta_1(\omega_s)$ [17]. For simplicity, this correction term is neglected. The dispersive wave is assumed to be initially Gaussian. The initial peak power and temporal width of the soliton and the dispersive wave were extracted from the simulations performed using the full nonlinear Schrödinger equation (see Fig. 4). The evolution of the spectrum of the dispersive wave obtained by solving Eq. (3) is illustrated in Fig. 8 as the soliton walks through the dispersive wave in the time domain.

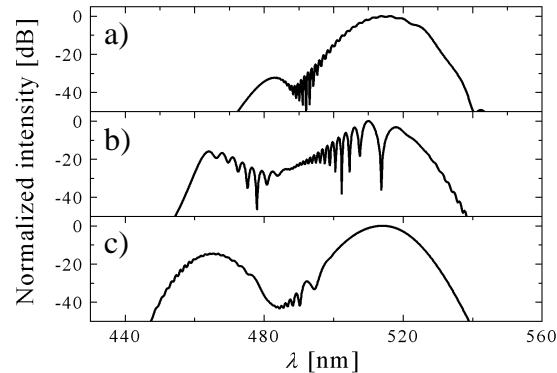


Fig. 8. Simulated spectrum of the dispersive wave for increasing propagation length using Eq. (3). a) $z = 5$ cm, b) $z = 10$ cm, and c) $z = 20$ cm.

The model, though simple, reproduces qualitatively all the features mentioned in the previous discussion. In particular, blue-shifted components appear as the soliton walks through the dispersive wave. Also, the gap between the spectrum of the dispersive wave and the new spectral components increases. Omission of the dispersion term in Eq. (3) results in an unchanged spectrum for the dispersive wave. This can be readily understood since, in that case, the soliton walks through the dispersive wave in a symmetric manner and, consequently, the blue chirp induced by the soliton's trailing edge is fully compensated for by the red chirp generated by the leading edge. Thus, we conclude that the observed enhancement of the

spectrum on the blue side of the SC finds its origin in XPM with a strong influence caused by the SSFS and the dispersive effects and that it does not result from a pulse trapping mechanism.

4. Discussion

Most of the literature on supercontinuum generation in MFs reports on experiments performed by launching pulses with a temporal width on the order of 100 fs and a wavelength located in the anomalous dispersion region of the fiber [1,3-7,11]. In these experiments, several authors have noticed an unexpectedly high amplitude [11] and large bandwidth of the dispersive wave spectral components [3]. Furthermore, it has also been observed that the magnitude of the gap between the pump wavelength and the blue spectral components increases with the fiber length [18]. It has also been pointed out that for increasing input power, the center wavelength of the blue band shifts further towards the blue wavelengths while its bandwidth narrows [3,11]. These observations can also be explained in the context of XPM.

Figure 9 displays spectra obtained by launching 140 fs pulses from an 80 MHz repetition-rate Ti:Sapphire laser (Spectra Physics/Tsunami) into 1 m of the MF described above at different input powers.

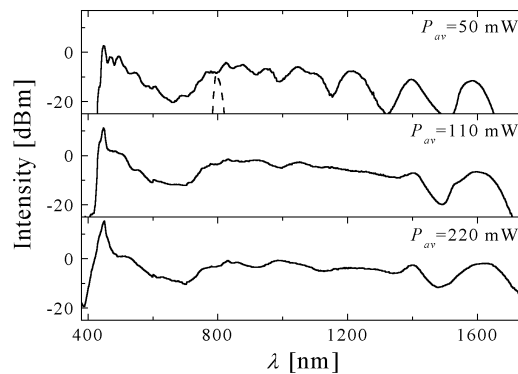


Fig. 9. Experimental spectra as a function of input power recorded at the output of 1 m of the same MF as in Fig. 2. $\lambda_p=800$ nm, and $\Delta\tau=140$ fs. The dashed line represents the spectrum of the input pulse.

The magnitude and bandwidth of the blue components, respectively, increases and broadens as the input power is increased. The simulated spectrogram of the SC illustrated in Fig. 9 for a 50 mW power is shown in Fig. 10. The initial pulse decays into multiple solitons that experience the SSFS. Simultaneously, several dispersive waves are generated. The solitons interact with the dispersive waves through XPM as described above, which leads to energy transfer from the red side of the dispersive waves to the blue side. Consequently, the spectral components of the dispersive waves appear shifted towards the blue for longer MFs and the gap between the pump and the spectral components of the dispersive waves is increased. Also, all the XPM interactions between the solitons and dispersive waves contribute to the growth of the blue band of the continuum. The temporal width of the main blue component exceeds 5 ps which is in agreement with recent experiments considering the longer fiber employed here [19]. Note that the strong modulation of the blue light was not observed in the autocorrelation measurements presented in Ref. [19]. This is probably due to the limited temporal resolution of the measurements and to the shot to shot variation which tends to average out the modulation.

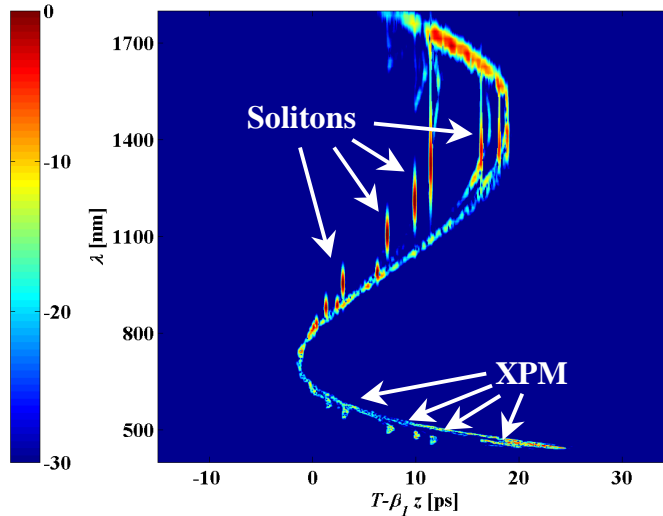


Fig. 10. Simulated spectrogram of the continuum after 50 cm of propagation. $\lambda_p=800$ nm, $P_{av}=50$ mW and $\Delta\tau=140$ fs. The parameters of the fiber are the same as the ones of Fig. 5.

5. Conclusion

Effects of cross-phase modulation within the continuum generated by launching sub-30 fs pulses from a 1 GHz Ti:Sapphire oscillator into a microstructured fiber were investigated. It was shown that the XPM interaction between the soliton and the blue dispersive wave results in an enhancement of the bandwidth of the continuum towards the blue wavelengths due to the sign of the group velocity mismatch between the soliton and the dispersive wave. The high dispersion value of the fiber at blue wavelengths was found to play a critical role in the process. The effects of cross-phase modulation in the case of supercontinua generated by 200 fs pulses were also discussed.

Acknowledgments

This work has been financially supported by the Academy of Finland, the graduate school in Electronics, Telecommunications and Automation (GETA), and the internal HUT graduate school on Information Technology. R. Kristiansen from Crystal Fibre A/S is acknowledged for kindly providing the MF. We are also grateful to K. P. Hansen from Crystal Fibre A/S for providing the parameters of the fiber and Mikko Merimaa for his help with the measurements.